Role of ZrO<inf>2</inf> and CeO<inf>2</inf> support on the In<inf>2</inf>O<inf>3</inf> catalyst activity for CO<inf>2</inf>

Fuel 331 (2023) 125878

Contents lists available at ScienceDirect

Fuel

journal homepage: www.elsevier.com/locate/fuel

Role of ZrO_2 and CeO_2 support on the In_2O_3 catalyst activity for CO_2 hydrogenation

Poonam Sharma, Phuoc Hoang Ho, Jieling Shao, Derek Creaser *, Louise Olsson

Chemical Engineering, Competence Centre for Catalysis, Chalmers University of Technology, SE-412 96 Gothenburg, Sweden

ARTICLE INFO

Keywords:
CO_2 hydrogenation
methanol
ZrO_2
CeO_2
In_2O_3

ABSTRACT

Methanol synthesis from CO_2 hydrogenation has drawn global attention as catalytic CO_2 hydrogenation is an attractive choice to mitigate CO_2 emissions and lessen dependency on fossil resources. In the present study, we have synthesized ZrO_2 and CeO_2-supported In_2O_3 catalysts for methanol synthesis from CO_2 hydrogenation and the catalytic performances of In_x/ZrO_2, and In_x/CeO_2 (x = 1 % and 13 %) were compared. Specifically, the effect of the ZrO_2 and CeO_2 supports on In_2O_3 catalyst during CO_2 hydrogenation was explored. This study reveals that ZrO_2 support increased the catalytic activity while the CeO_2 support decreased although both supports have almost the same indium loading and surface area. Various characterizations like XRD, DRIFT, CO_2-TPD, H_2-TPR and XPS analysis of catalysts provided insight into changes that arise after mixing the two oxides and during the reaction as well as after the reaction. The stabilities of In_2O_3, In_{13}/ZrO_2, and In_{13}/CeO_2 were tested for up to 50 h and we found In_{13}/ZrO_2 was stable during this time-on-stream, while In_{13}/CeO_2 lost activity after 2 h of reaction. XPS results of spent catalysts showed that $In(OH)_3$ was observed significantly over the spent In_{13}/CeO_2. OH groups were also verified by DRIFT experiments, however at low levels due to low CO_2 conversion at atmospheric pressure. XRD analysis confirmed the sintering of CeO_2 support during the reaction. Thus, the hydrophilic nature of CeO_2, redox properties of CeO_2 and sintering of CeO_2 support in the presence of water, were the main reasons for the early deactivation of In_{13}/CeO_2. A regeneration study was carried out to regenerate the catalyst and the results showed that partial regeneration of the In_{13}/CeO_2 catalyst is possible by Ar flushing. We, therefore, suggest that the build-up of OHgroups deactivate the In_{13}/CeO_2 catalyst and some of these OH groups could be removed during flushing with inert gas, causing a partial regeneration. However, the decreased surface area is not reversible, and this results in a continuous decrease in the activity of the catalyst after repeated experiments, even if the catalyst is flushed with Ar between the experiments.

1. Introduction

The excessive use of fossil fuels increases the emissions of CO_2 into the atmosphere which contributes to global warming.[1,2] A combined process of CO_2 capture, storage and utilization is an important way to mitigate the surplus CO_2 and dependency on fossil fuels.[3,4] Thus, production of chemical feedstocks and transportation fuels from the utilization of CO_2 has attracted great attention recently.[5] Methanol is an important chemical feedstock which is used in various applications and can be further converted into other important chemicals such as chloromethane, methyl tert-butyl ether, formaldehyde, acetic acid, and fuels.[6,7] Methanol can be synthesized from various reactions where CO_2 hydrogenation is an environmentally important chemical reaction. It usually occurs with the following system of competing and series reactions as shown in Scheme 1.

CH_3OH synthesis from CO_2 and CO hydrogenation are exothermic (Eq.1 and 2), whereas Eq. 3, the competitive reverse-water-gas-shift reaction (RWGS), is endothermic during the CO_2 hydrogenation.[6] Additionally, the conversion of methanol into hydrocarbons is also an attractive solution to provide alternative sustainable energy resources. [7]

Over the decades, $Cu/ZnO/Al_2O_3$ and Cu-ZnO catalysts have been used and studied for the synthesis of CH_3OH from syngas at industrial and laboratory scales, respectively. Similarly, a wide variety of heterogeneous catalysts are developed for the synthesis of CH_3OH from CO_2 hydrogenation [7] where transition metal catalysts like Cu, Pd, Ag, and Pt are used.[8] Recently, oxide-based catalysts like In_2O_3,[9,10] metal promoted In_2O_3,[11,12] and ZnO-ZrO_2[13] have been reported to have

* Corresponding author.
E-mail address: creaser@chalmers.se (D. Creaser).

https://doi.org/10.1016/j.fuel.2022.125878
Received 14 April 2022; Received in revised form 24 August 2022; Accepted 29 August 2022
Available online 12 September 2022

$$CO_2 + 3H_2 \rightleftharpoons CH_3OH + H_2O \quad \Delta H = -49.5\ kJ\ mol^{-1} \quad (1)$$

$$CO + 2H_2 \rightleftharpoons CH_3OH \quad \Delta H = -90.4\ kJ\ mol^{-1} \quad (2)$$

$$CO_2 + H_2 \rightleftharpoons CO + H_2O \quad \Delta H = +41.5\ kJ\ mol^{-1} \quad (3)$$

Scheme 1. Possible reactions for the synthesis of methanol.

excellent activity for methanol synthesis (Table S1, See supporting information).[14-16] The oxide-based catalysts have different active sites than traditional metal catalysts with different reaction mechanisms.[17] Martin et al. synthesized ZrO_2 supported In_2O_3 which rendered 100 % selectivity for CH_3OH synthesis and was found to be stable up to 1000 h on stream whereas the reference Cu-ZnO-Al_2O_3 catalyst lost 44 % of its activity in 100 h.[18] Recently, In_x/ZrO_2 (x = 0.1-5 wt%) catalysts were screened for CH_3OH synthesis under industrially relevant conditions and a highly tunable selectivity for CH_3OH from CO_2 hydrogenation was observed.[19] Loadings of 2.5-5 wt% In on catalysts have shown 70-80 % CH_3OH selectivity whereas 0.1 wt% loading of In exhibited a CO selectivity up to 80 %. In addition, the distribution of products was found to depend on the interfacial structure of ZrO_2 and In_2O_3. A composition of Cu-In-Zr-O was reported to act as a bifunctional catalyst, where In_2O_3 adsorbs CO_2 and the Cu-sites adsorb, and provide active hydrogen to adjacently adsorbed CO_2.[20]

Generally, high pressure and low temperature favor the synthesis of CH_3OH. However, a high reaction temperature aids CO_2 activation whereas a lower temperature is thermodynamically favorable for CH_3OH formation and this condition creates a kinetic limitation for the reaction.[21] At the reaction condition, other competing reactions occur in parallel in addition to the RWGS that can produce many side products like methane, formaldehyde, and formic acid.[22-25] The support materials play a significant role in heterogeneous catalysis.[8] In an interesting study by Hartadi et al., the authors have discussed the importance of support materials like Al_2O_3, ZnO, ZrO_2, and TiO_2 for CO_2 hydrogenation.[26] Due to the versatile properties and weak hydrophilic character of ZrO_2, over the past decades, substantial progress has been made over ZrO_2-supported catalysts.[27-30] It has been stated that ZrO_2 supports interact with metals and oxide-based catalysts and change various reaction parameters and environments which increased the activity of the catalysts.[31] Perez-Ramirez et al. studied the role of ZrO_2 as a support for In_2O_3 in CO_2 hydrogenation to methanol and suggested that the ZrO_2 support used its own oxygen vacancies to activate the CO_2.[32] The study was mainly focused on ZrO_2 whereas other supports like Al_2O_3 and CeO_2 were used for a comparison study. Gong et al. described the strong electronic interaction between In_2O_3 and ZrO_2 which was responsible for high selectivity towards methanol.[25] Previously, the promotional effect of CeO_2 on Ga_2O_3 was studied experimentally for the RWGS and it was observed that the CeO_2 increased the oxygen vacancies which increased the dissociation of absorbed H_2 to react with absorbed CO_2 and increase coverages of bicarbonate species.[33] Moreover, ceria can enhance the oxygen storage and release in oxidizing and reducing conditions, respectively.[34-36] In another study, In_2O_3/CeO_2 was studied for the RWGS and maximum CO_2 conversion of 20 % was reported when In_2O_3 and CeO_2 were mixed in a 1:1 weight ratio at 773 K.[37] However, this study has not discussed the formation of methanol over In_2O_3/CeO_2 catalysts. Thus, most studies have focused on CO formation over CeO_2 supported catalysts.

Although studies reported the positive effect of ZrO_2 as a support for methanol synthesis,[31] less attention has been paid to CeO_2 as a support which is also capable of promoting the formation of oxygen vacancies for CO_2 activation. Therefore, these studies intrigued us to explore more about CeO_2 as a support for CO_2 hydrogenation into methanol along with ZrO_2. Thus, a comparative study was carried out between In_x/ZrO_2 and In_x/CeO_2 to identify the influence of the catalyst support on catalyst activity, deactivation, and stability during CO_2 hydrogenation to methanol while having comparable quantities of oxygen vacancies, In_2O_3 loadings and surface areas. To the best of our knowledge, there is no report where deactivation and regeneration studies of CeO_2-supported In_2O_3 were explored, which is the objective of the current study.

2. Experimental Section

2.1. Materials

$In(NO_3)_3{\cdot}xH_2O$ salt was purchased from Sigma-Aldrich. Supporting materials ZrO_2 (monoclinic phase, extrudates, SZ 31164, NORPRO), and CeO_2 powder (99.5 H.S.A 514, Rhône-Polenc, La Rochelle, France) were used. For activity tests in the reactor, the catalyst powders were pelletized into 250-500 μm particles using a hydraulic press after impregnation of indium oxide (In_2O_3) on zirconia (ZrO_2) and ceria (CeO_2).

2.2. Catalysts preparation

The catalysts (In_x/ZrO_2 & In_x/CeO_2, x = 1 and 13 wt% In loading) were prepared by incipient wetness impregnation using CeO_2 and ZrO_2 as supports for In_2O_3 loading (Figure S1). For that, the $In(NO_3)_3{\cdot}xH_2O$ salt was dissolved in a mixture of ethanol and MilliQ water and dropwise added directly to the powder support to form a slurry. Further, the slurry was dried at 373 K and then the powder was calcined at 573 K in a furnace for 3 h. A similar procedure was used for the preparation of In_x/CeO_2. Note that to determine the role of the supports, unsupported bulk In_2O_3 was prepared using a calcination process where the Indium salt was calcined at 573 K in the furnace for 3 h. Further, catalytic CO_2 hydrogenation was conducted in a continuous reactor setup. Prior to the reaction, a thermal treatment was done in which the catalyst was heated in pure Ar (30 mL min^{-1}) at 573 K and 0.5 MPa for 1 h.

2.3. Characterization

To determine the crystalline nature of the catalysts, powder X-Ray diffraction (XRD) measurements were performed in a SIEMENS diffractometer D5000 using Cu Kα radiation (λ = 1.5418 Å) with a tube current and voltage of 40 mA and 45 kV, respectively. Diffraction patterns were collected with 2θ ranging from 20° to 70° using a step size of 0.02.

In-situ FTIR spectroscopy experiments were performed in diffusive reflectance (DRIFT) mode with a BRUKER Vertex 70 spectrometer equipped with a nitrogen-cooled MCT detector and a high-temperature stainless steel reaction cell (Harrick Praying Mantis™) with KBr windows. To measure the temperature of the sample, a K-type thermocouple was fitted into the sample holder and controlled by a PID regulator (Eurotherm). The total flow of gases into the reaction cell was fixed at 100 ml min^{-1} in all experiments by feeding the gases via individual mass flow controllers. Spectra were recorded by accumulating 265 scans in the range of 4000–600 cm^{-1} with a resolution of 4 cm^{-1} for the temperature range of 493-553 K at atmospheric pressure. Time-resolved spectra were recorded every 60 s to obtain phase-resolved spectra.

The specific surface area of the catalysts was determined by nitrogen sorption at 77 K (Micromeritics Tristar 3000) using the Brunauer–Emmett– Teller (BET) method. The samples were dried in N_2 flow at 500 K for 3 h prior to the measurements.

X-ray photoelectron spectroscopy (XPS) was conducted using a Physical Electronics (PHI) 5000 VersaProbe III Scanning XPS Microprobe featuring focused monochromatic Al-Kα radiation with the X-ray (E = 1486.6 eV) beam size around 100 μm. The X-ray was generated via the electron beam bombardment onto the Al anode which was operating at 15 kV and 25 W. A hemispherical capacitor electron-energy analyzer was used equipped with a 32-channel plate and a position-sensitive detector. The samples were adhered onto double-sided tapes, fastened to the sample plate, and then introduced into the spectrometer after a

prolonged pre-pumping process in the introduction chamber. Due to the poor-conducting/insulating nature of the powder samples, charge compensation was conducted under the operation of both the electron neutralizer and ion gun. The measurements were run under a UHV environment around 1.0-3.0 $\times 10^{-6}$ Pa. The take-off angle of the emitted photoelectron is 45° and the analyzer was operated in the constant pass energy mode (Survey: 280 eV; Regional/Narrow scan: 26 eV).

X-ray fluorescence (XRF) spectroscopy was carried out using a WDXRF (Wavelength Dispersive X-ray Fluorescence) spectrometer equipped with a Rh source operated at 60 kV and 125 mA.

TEM measurements were performed on a Titan 80-300 system (FEI Company) operated at 300 kV. The sample was crushed between two glass slides and distributed over a perforated carbon Cu grid to prepare the sample for TEM analysis.

CO_2 temperature-programmed desorption (CO_2-TPD) and H_2 temperature-programmed reduction (H_2-TPR) were studied using a digital scanning calorimeter (Sensys DSC, Setaram) coupled with a mass spectrometer (HPR-20 QUI, Hiden). For CO_2-TPD, 50 mg of powder catalyst was loaded into a microreactor and then pretreated with Ar at 573 K for 30 min. Thereafter, the microreactor was cooled to 313 K and exposed to a flow of 5000 ppm CO_2/Ar for 90 min. Further, the catalyst was purged with Ar for 60 min. Then, the CO_2 desorption behavior was studied in Ar by increasing the temperature from 313 K to 973 K with a ramp rate of 10 K/min. The concentration of CO_2 was monitored using the mass number of m/z = 44. For H_2-TPR measurements, the catalyst (30 mg) was pretreated in Ar at 573 K for 30 min and then cooled to 298 K. The H_2 flow (20 NmL/min, 1 vol% H_2/Ar) was introduced at 298 K for 20 min and then the temperature was ramped up to 1073 K (10 K/min) and maintained for 30 min at this temperature. The concentration of H_2 was monitored using the mass number of m/z = 2.

2.4. Catalytic activity test

The CO_2 hydrogenation reaction was evaluated in a continuous high-pressure fixed bed vertically positioned tubular stainless-steel reactor (0.85 cm diameter and 21.45 cm length) supplied by Vinci Technologies, France. The reactor was loaded with 0.5 g of catalyst sample. Reaction conditions were as follows: $H_2/CO_2 = 3$ (molar ratio), GHSV = 12000 h^{-1}, T = 493-573 K and P=3.0 MPa. The packing of the reactor consisted first of a bottom layer of 10.3 cm of pure SiC, above which was placed a layer of pure catalyst of (ca. 0.7 cm), which was placed between two thin layers of quartz wool. Finally, the remaining upstream part of the reactor (ca. 10.5 cm) was filled with SiC. A thermocouple was positioned in the reactor with its tip in contact with the catalyst sample for measuring the actual catalyst temperature during the reaction. Prior to the reaction, the catalysts were pre-treated with pure Ar (30 NmL min^{-1}) at 573 K for 1 h under 0.5 MPa pressure. After that, the catalysts were cooled down to reaction temperature in pure Ar, and then the reactant gases (CO_2 and H_2 with a molar ratio of 1:3) were introduced into the reactor at a gas hourly space velocity (GHSV) of 12000 h^{-1} and the pressure was raised to 3.0 MPa. Catalytic activity was measured at temperatures ranging from 493 to 573 K. The Ar flow was resumed after each day of measurements and maintained overnight. The catalyst bed remained in a temperature range from the desired reaction temperature to room temperature. Measurements were recorded when the reaction reached a steady state. The concentrations of the gaseous products in the outlet streams were measured by an on-line gas chromatograph (GC, SCION 456) equipped with a flame ionized detector (FID), and a thermal conductivity detector (TCD). The TCD detector was connected to an HS-Q column whereas the FID was connected to a mild-polar aluminum oxide packed column (Agilent Technologies, Inc., HP-Al/S, 30*0.53 mm, 15 μm) for product separation.

The CO_2 conversion (X_{CO2}), selectivities for CH_3OH (S_{CH3OH}), CO (S_{CO}), and CH_4 (S_{CH4}) , and space-time-yield (STY) were calculated according to the following equations:

$$XCO2 = \frac{FCO2,\text{in} - FCO2,\text{out}}{FCO2,\text{in}} \times 100\,\% \quad (4)$$

$$SCH3OH = \frac{FCH3OH,\text{out}}{FCO2,\text{in} - FCO2,\text{out}} \times 100\,\% \quad (5)$$

$$SCO = \frac{FCO,\text{out}}{FCO2,\text{in} - FCO2,\text{out}} \times 100\,\% \quad (6)$$

$$SCH4 = \frac{FCH4,out}{FCO2,in - FCO2,out} \times 100\% \quad (7)$$

$$STY = \frac{FCH3OH*M}{Wcat} \quad (8)$$

where F_i is the molar flow rate of component i, M is the molar mass of methanol and W is the weight of the catalyst sample.

3. Results

3.1. Catalyst characterization

Table 1 shows the In contents of four catalysts from XRF measurements. The In loadings were close to the targeted values of 1 and 13 wt %. A similar loading of In for each pair of catalysts using different supports ZrO_2 and CeO_2 allows for comparing the properties and the activity of the samples.

The crystallinity of CeO_2 and ZrO_2-supported In_2O_3 catalysts were studied using XRD analysis (Figure 1). The patterns of the unsupported bulk In_2O_3 showed four main reflections at 2θ = 30.5°, 35.4°, 50.9° and 60.5°, which are assigned to the diffractions from the (2 2 2), (4 0 0), (4 4 0) and (6 2 2) planes. The XRD patterns of the freshly prepared In_{13}/ZrO_2 showed the characteristic diffractions of cubic In_2O_3 and monoclinic ZrO_2.[38] It should be noted that a small shift in the diffraction peaks corresponding to In_2O_3 was observed, for example, the reflection of (2 2 2) was shifted from 30.5° to 30.9° (Figure S2a). These results suggest some changes in the coordination of In-O-In (Figure 2a). It has been reported that the ZrO_2 support helps to make In_2O_3 electronically rich which is favourable for methanol formation.[39] Previous studies have discussed such interactions between the support and catalyst.[25,32] In the pattern of In_{13}/CeO_2, the diffraction peaks of the CeO_2 support were observed at 2θ = 28.6°, 33.1°, 47.5° and 56.3°, which corresponds to the (1 1 1), (2 0 0), (2 2 0) and (3 1 1) planes of CeO_2.[40] However, it should be noted that the intensity of the diffractions of In_2O_3 is low for the In_{13}/CeO_2 sample, making the interpretation difficult. This is likely due to that the In_2O_3 is well dispersed and does not form large In_2O_3 crystallites. These results are supported by the STEM images, where the particles were not as clear as for the In_{13}/ZrO_2 sample. This will be further discussed in connection to Figure 3. The peaks of In_2O_3 on ZrO_2 support, on the other hand, are significantly stronger, suggesting larger crystallinity of In_2O_3 on the ZrO_2 support than on the CeO_2 support. The crystallite size of the bulk In_2O_3 was 19.5 nm for the (222) plane (2θ = 30.5°), whereas it was only 9.1 nm for In_{13}/ZrO_2. The crystallite size of In_2O_3 on CeO_2, was not possible to determine with accuracy because the diffraction peak was so small. The

Table 1
Porous and compositional properties of In_x/ZrO_2 and In_x/CeO_2.

Catalysts	In content		Porous properties[b]	
	Nominal (wt %)	Measured[a] (wt %)	A_{BET} (m^2/g)	V_{pore} (cm^3/g)
In_{13}/ZrO_2	13	11.9	60.0	0.21
In_{13}/CeO_2	13	13.5	66.6	0.13
In_1/ZrO_2	1	0.7	69.9	0.27
In_1/CeO_2	1	0.8	80.8	0.16
Bulk In_2O_3	-	-	5.0	0.02

[a]Determined by XRF. [b]Measured by N_2 adsorption.

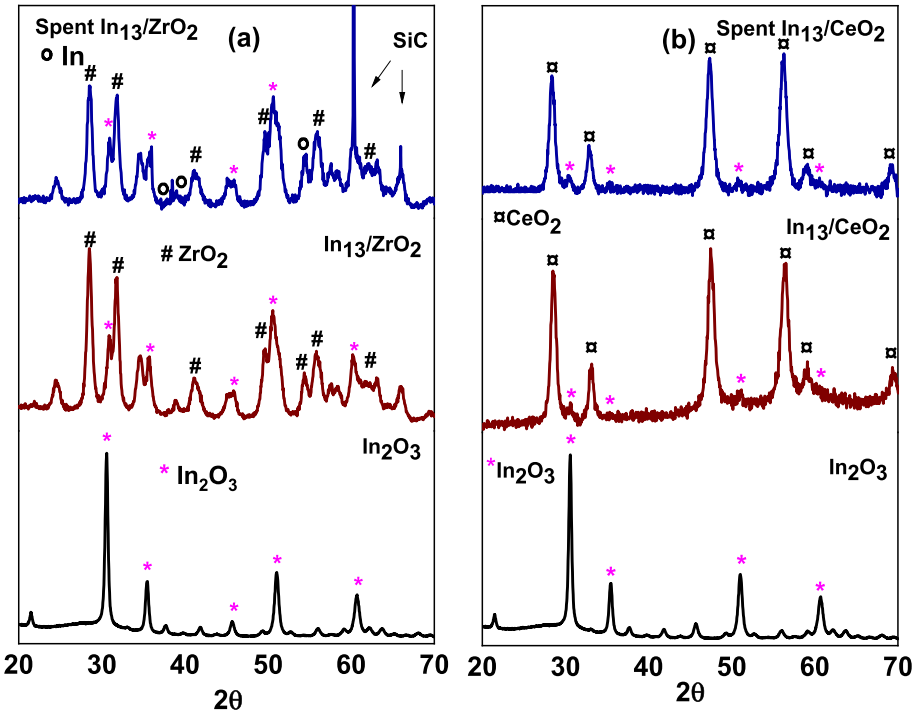

Figure 1. XRD patterns of (a) bulk In_2O_3 (black), In_{13}/ZrO_2 (red) and spent In_{13}/ZrO_2 (blue) and, (b) bulk In_2O_3 (black), In_{13}/CeO_2 (red) and spent In_{13}/CeO_2 (blue) catalyst.

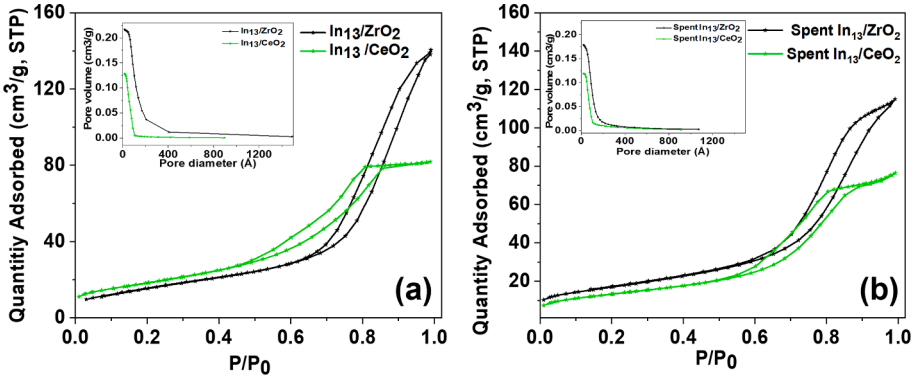

Figure 2. N_2 adsorption/desorption of In_{13}/ZrO_2, and In_{13}/CeO_2 for a) Degreened and b) Spent catalyst. The pore size distribution of the catalysts is presented in the inset.

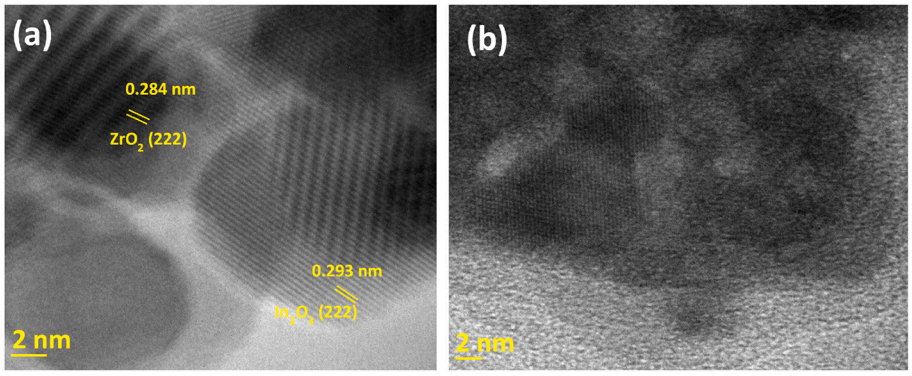

Figure 3. TEM analysis of (a) In_{13}/ZrO_2 and, (b) In_{13}/CeO_2.

results are in line with earlier reported studies where the size of In_2O_3 particles decreased after impregnation on CeO_2 and ZrO_2.[37] XRD patterns with negligible In_2O_3 peak intensities were found with 1 wt% loading of In on both supports (Figure S3).

The diffraction patterns of SiC were observed in the XRD in the case of the spent In_{13}/ZrO_2 catalyst since it was used as a filler while packing the reactor.[41,42] There was no change in the diffraction of In_2O_3 and ZrO_2 for the spent In_{13}/ZrO_2 which indicates no change in the crystalline structure of the catalyst after the reaction. However, small intensity peaks of In metal ($2\theta = 36.7°$, 39.1°, 54.4°, PDF#04-010-6206) were observed which was also detected in the XPS analysis of the spent In_{13}/ZrO_2 catalysts.[43]

The porosity of In_{13}/ZrO_2 and In_{13}/CeO_2 was measured using N_2 physisorption and the data is summarized in Table 1. The surface areas of In_{13}/ZrO_2 and In_{13}/CeO_2 were found to be 60.0 m^2/g and 66.6 m^2/g, respectively, whereas the surface area of the unsupported bulk In_2O_3 catalyst was only about 5 m^2/g. The surface area and pore volume increased when the In loading was decreased from 13 % to 1 % over ZrO_2 and CeO_2 (Table 1 and Figure 2 and Figure S4). The pore volume of the ZrO_2-supported catalysts was found to be larger than that of CeO_2-supported catalysts while the opposite was true for surface areas. It was observed that the surface area and pore volume decreased after loading of In on both supports. The results indicate that the loading of In_2O_3 blocks some of the pores of the support. It is also noted that the average pore width was larger for ZrO_2 than for the CeO_2 support. A larger pore size of ZrO_2 than CeO_2 could explain the larger crystallite size of In_{13}/ZrO_2 than In_{13}/CeO_2.

Type IVa N_2-Isotherms were observed for all catalysts (Figure 2), which is characteristic of mesoporous materials.[44] The CeO_2-supported In_2O_3 catalysts show a hysteresis loop of type H1 which is associated with porous materials exhibiting a narrow distribution of relatively uniform pores while a type H3 loop was observed for ZrO_2-supported In_2O_3 catalysts [44]. The surface area and In contents of all the supported catalysts are similar which is favorable to compare their catalytic performance. Only the bulk In_2O_3 sample had a far lower surface area and pore volume.

The surface area of spent In_{13}/ZrO_2 and In_{13}/CeO_2 were also measured, and it was found that the surface area of In_{13}/CeO_2 was reduced from 66.6 to 48.0 m^2/g, whereas no change was observed in the surface area of In_{13}/ZrO_2 (Figure 2b). The pore volumes decreased of both spent In_{13}/ZrO_2 (from 0.21 to 0.17 cm^3/g) and In_{13}/CeO_2 (from 0.13 to 0.11 cm^3/g) which indicates blockage of pores.

TEM imaging of In_{13}/ZrO_2 and In_{13}/CeO_2 are shown in Figure 3. It demonstrates that the crystalline In_2O_3 particles are well distributed on the surface of the crystalline ZrO_2 (Figure 3a). While on the CeO_2 support, In_2O_3 particles might be embedded between CeO_2 layers that cover the crystalline planes of In_2O_3. Thus, the crystalline planes for In_2O_3 were difficult to distinguish. These results are consistent with the XRD patterns where the diffraction of indium was very weak (Figure 1b). The uniform distribution of In_2O_3 over CeO_2 and ZrO_2 was observed in EDX mapping of both catalysts (Figure S5)

To examine the chemical state of the elements, XPS analyses of In_2O_3, In_{13}/ZrO_2, and In_{13}/CeO_2 were carried out (Figure 4-5, Figure S6). Before each analysis, all samples were *ex situ* pretreated in Ar at 573 K for 1 h. The O 1s core level of the unsupported In_2O_3 catalyst was deconvoluted into three peaks at 531.7, 530.9 and 529.2 eV which were assigned to surface OH, defect (vacancy), and lattice (In-O-In), respectively (Figure 4a).[45] For the supported catalyst, it is more complicated to make the deconvolution because each component of the core O 1s is also contributed by the support. Moreover, the interaction between In_2O_3 and the support can cause a change in the electron density around O, which possibly makes a shift in the position of the peaks. In_{13}/ZrO_2 revealed three pronounced O 1s peaks at 533.0, 531.0, and 529.7.0 eV (Figure 4a). The peaks at about 529.7 and 533.0 eV correspond to $O_{lattice}$ and OH, respectively, while that at 531.0 eV is related to the oxygen defects.[46] In the case of the In_{13}/CeO_2 catalyst, four peaks of O 1s at 528.8, 530.2, 531.3, and 533.0 eV are assigned to the binding energies of Ce^{4+}-O, oxygen defects (Ce^{3+}-O), In-O-In and OH, respectively (Figure 4b).

It is seemingly difficult to identify the contribution of support material in the total amount of oxygen defects as peaks are overlapped after deconvolution. To better understand the contribution of the support, the core level of Zr 3d and Ce 3d were deconvoluted and the data are summarized in Figure 5. As shown in Figure 5a, the Zr 3d core level was deconvoluted into three doublets at 181.8 , 183.3 , and 185.2 eV. The binding energies at 181.8 and 183.3 eV were assigned to ZrO_2 and Zr $(OH)_4$, respectively [47], while the higher binding energy at 185.2 eV could be from changed forms of ZrO_2 due to synergic interaction with In_2O_3 (In-O-Zr, Figure 5a).[25,48,49] The spectrum of Ce 3d core level was deconvoluted into two series of bands u and v, corresponding to the

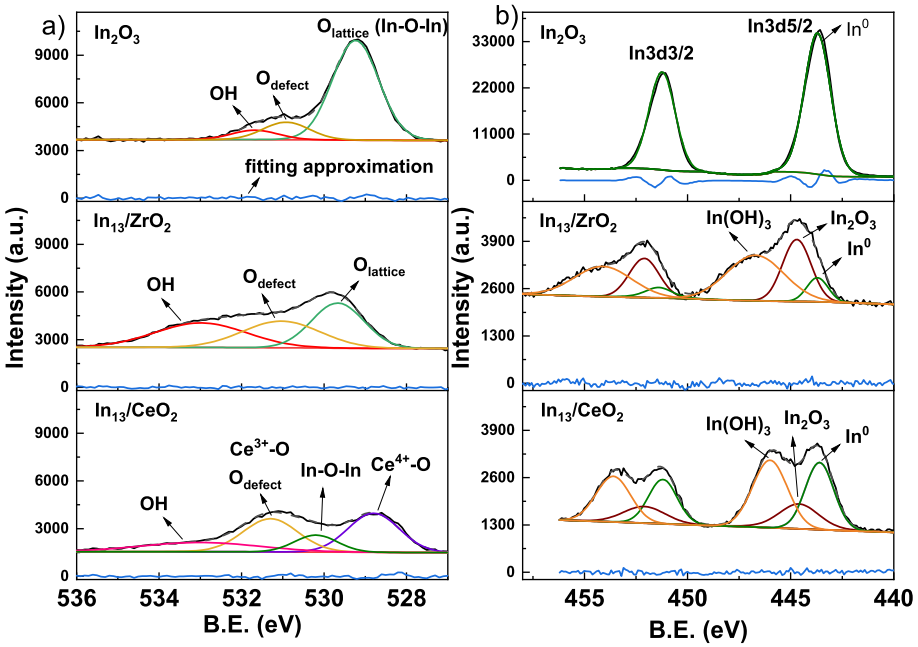

Figure 4. XPS analysis of (a) O 1s of In_2O_3, In_{13}/ZrO_2 and In_{13}/CeO_2 and, (b) In3d of In_2O_3, In_{13}/ZrO_2 and In_{13}/CeO_2.

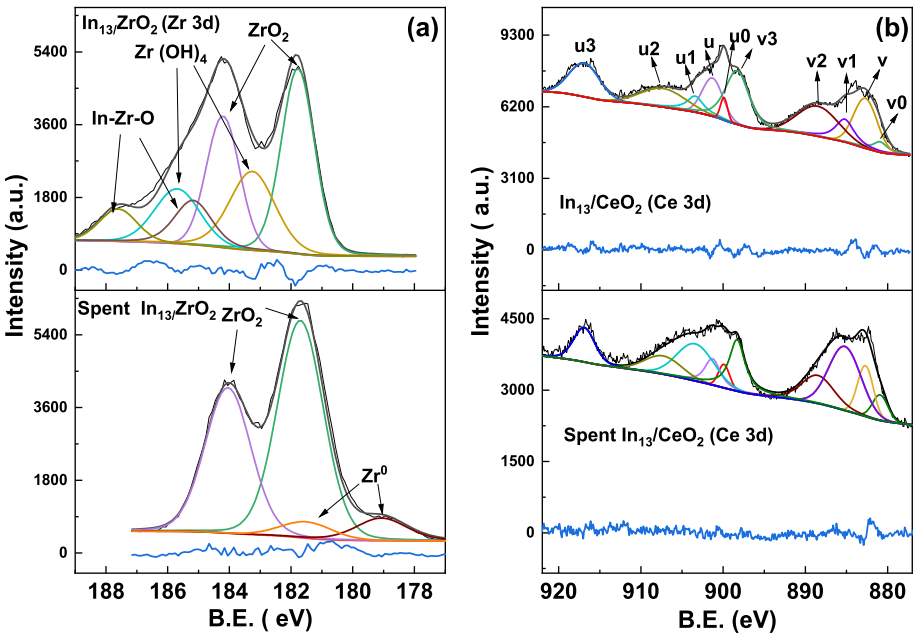

Figure 5. XPS analysis of (a) Zr 3d of In_{13}/ZrO_2 and spent In_{13}/ZrO_2, (b) Ce 3d of In_{13}/CeO_2 and spent In_{13}/CeO_2.

3d3/2 and 3d5/2 spin-orbits, respectively (Figure 5b). The group of six peaks denoted as v, v2, v3, u, u2, and u3 was assigned for the oxidation state of +4 (Ce^{4+}) whereas the group of four peaks labeled as v0, v1, u0, and u1 was characteristic of the oxidation state of +3 (Ce^{3+}).[50] The oxidation state of +4 (Ce^{4+}) is dominant (82 %) in the In_{13}/CeO_2.[51,52 53]

Figure 4b shows the binding energy of In3d core levels of In_2O_3, In_{13}/ZrO_2 and In_{13}/CeO_2 catalysts. Two peaks located at 443.6 and 451.3 eV were observed in the XPS spectra for the unsupported bulk In_2O_3, which can be attributed to the characteristic spin-orbit splits 3d5/2 and 3d3/2 of In 3d core level. [48,49] Both peaks are associated with indium as the catalyst was prepared by thermal composition and was unsupported. The binding energy of 3d5/2 at 443.7 eV is rarely reported in the literature for oxide forms of indium. Instead, the peak at 443.7 eV and 444.8 eV have been usually reported for In^0 and In^{3+}, respectively.[54] Therefore, the unusual characteristics of the 3d5/2 binding energy of the unsupported In_2O_3 catalyst could be related to the nature of the material prepared by the decomposition of $In(NO_3)_3$ precursor. It can be noted that metallic In was not detected by the XRD analysis (Figure 1). The metallic indium could either have been formed during heating of the salt in the preparation, and/or possibly by reduction of the surface under the ultra-high vacuum environment of the XPS instrument. In addition, XPS is a surface analysis technique, whereas XRD measures bulk properties. So metallic In is apparently only present on the surface of the materials. For the supported catalysts, the In 3d spectrum was deconvoluted into three doublets assigning to metallic In, In_2O_3, and $In(OH)_3$ (Figure 4b). The percentage of surface In_2O_3 was slightly higher on In_{13}/ZrO_2 (36.2 %) than In_{13}/CeO_2 (31.1 %). A core level of 3d5/2 of In3d was observed in both supported catalysts at 446.0 eV for In_{13}/CeO_2 and 446.7 eV for In_{13}/ZrO_2 (Figure 4b), which are due to $In(OH)_3$.[55] This peak was higher in the case of In_{13}/ZrO_2 (53.3 %) than In_{13}/CeO_2 (41.3 %). These results indicate that the amount of $In(OH)_3$ is higher over fresh In_{13}/ZrO_2 than In_{13}/CeO_2 which is also the same trend as the percentage of the OH fraction from the O 1s core level data. The metallic species of In with the binding energy of 3d5/2 at 443.7 eV were also observed in both supported catalysts and their percentage were 27.5 % and 10.5 % over In_{13}/CeO_2 and In_{13}/ZrO_2, respectively.

Deconvolutions of the XPS spectra of spent catalysts were carried out to interpret the changes in the chemical state of In and supports after the reaction (Figure S6 and Table 2). For that, the spent catalysts were flushed with Ar during the cooling down of the catalyst bed after the reaction and thereafter exposed to air at room temperature before the XPS measurements. XPS analysis showed 31 % oxygen vacancies over fresh In_{13}/ZrO_2 whereas it was 34 % over In_{13}/CeO_2. Further, the percentage of oxygen vacancies increased from 34 to 39 % over the spent In_{13}/CeO_2 while it dropped from 31 to 19 % in the case of In_{13}/ZrO_2. The chemical state and amount of metal hydroxide were also examined in spent and fresh catalysts, and it was found that the amount over ZrO_2 also increased from 60 to 90 % in the spent In_{13}/ZrO_2 (Figure 5a). A smaller peak, with a binding energy of around 179 eV was also observed in the spent In_{13}/ZrO_2 (Figure 5a), which could be associated with Zr 3d5/2 for metallic Zr.[47] The amount of Ce^{3+} ion increased from 18 to 45 % in the spent In_{13}/CeO_2 (Figure 5b). This result indicates that the CeO_2 support creates more oxygen vacancies in an H_2 environment. Moreover, the percentage of $In(OH)_3$ (determined from the In3d core level) was reduced from 41.3 to 30.8 % over the spent In_{13}/CeO_2 whereas it became zero from 53.3 % over the spent In_{13}/ZrO_2 (Figure S6, Table 2). We also observed a change in the ratio of In^0/In_2O_3 after the reaction. It increased from 0.29 to 0.65 for the In_{13}/ZrO_2 whereas it decreased from 0.88 to 0.34 for the In_{13}/CeO_2. The data suggest that during the reaction, the oxidation states changed not only for the active phase (In^0/In_2O_3) but also for the supports.

Table 2
XPS analysis of In_{13}/ZrO_2, In_{13}/CeO_2, spent In_{13}/ZrO_2 and spent In_{13}/CeO_2.

Chemical state	ZrO_2 (%) from Zr 3d	Oxygen defects (%) from O 1s	In $(OH)_3$ (%) from In 3d	Ce^{3+} state (%) from Ce 3d
In_{13}/ZrO_2	60	31	53.3	-
Spent In_{13}/ZrO_2	90	19	0	-
In_{13}/CeO_2	-	33	41.3	18
Spent In_{13}/CeO_2	-	39	30.8	45

3.2. *Characterization of the interaction of gas-phase species with the catalyst surface*

In-situ DRIFT spectroscopy was conducted to study the adsorption behavior of CO_2 and identify the adsorbed species during the interaction of CO_2 with H_2 over In_{13}/ZrO_2, and In_{13}/CeO_2 (Figures 6-7). Prior to each

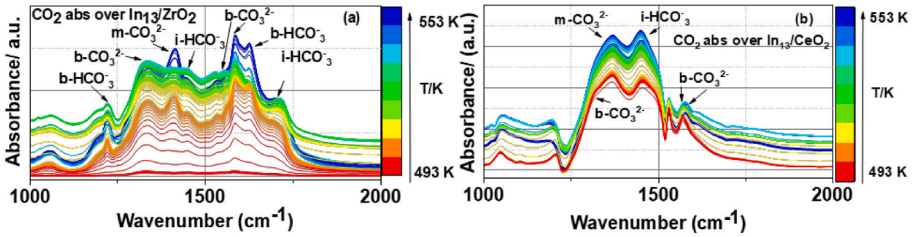

Figure 6. CO_2 adsorption study over (a) In_{13}/ZrO_2 and, (b) In_{13}/CeO_2.

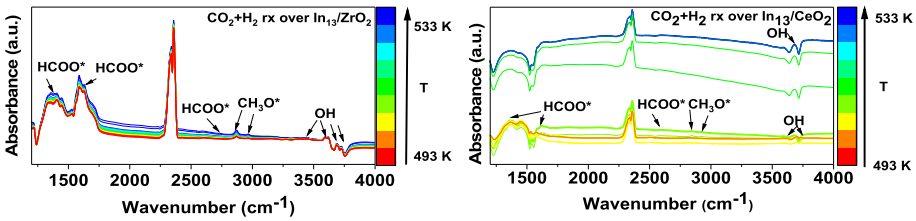

Figure 7. CO_2+H_2 reaction study over (a) In_{13}/ZrO_2 and, (b) In_{13}/CeO_2.

experiment, the catalysts were pre-treated at 573 K in Ar for 1 h. After pretreatment, the catalyst was cooled down in Ar to the desired temperature where the background spectrum was collected at 493 K. The catalyst was thereafter exposed to a steady gas flow of 0.03 vol.% CO_2 in Ar at 493 K and the adsorption behavior of CO_2 for In_{13}/CeO_2 and In_{13}/ZrO_2 catalysts are shown in Figure 6. Bands related to ionic bicarbonate (i-HCO_3^-)[56] as well as bridged bicarbonate (b-HCO_3^-)[56] were observed on the surface of In_{13}/ZrO_2. The bands related to b-HCO_3^- appeared at 1620 and 1225 cm^{-1} while for i-HCO_3^- the bands were found at 1695 and 1435 cm^{-1} (Figure 6a).[57] Bands related to carbonates were also observed at 1585, 1555 and 1335 cm^{-1} for b-CO_3^{2-} and 1375 cm^{-1} for monodentate carbonate (m-CO_3^{2-}).[57] The peak intensity of b-HCO_3^- species was higher than those of i-HCO_3^- at 553 K for In_{13}/ZrO_2. Additionally, the b-CO_3^{2-} and m-CO_3^{2-} species bands were more intense than the bicarbonate bands at this temperature. Thus, the features for carbonate species are much stronger than those for bicarbonate species at higher adsorption temperatures.[56] The CO_2 absorption bands observed on In_{13}/CeO_2 at 1575 and 1315 cm^{-1} suggest the presence of b-CO_3^{2-} at 493 K. When the temperature increased from 493 to 553 K, the b-CO_3^{2-} species began to disappear or their intensity decreased on the surface of In_{13}/CeO_2, whereas the m-CO_3^{2-} and i- HCO_3^- species at 1375, and 1448 cm^{-1}, were detected at 553 K (Figure 6b). [32]

In addition, time and temperature resolved spectra were collected during the introduction of 0.09 vol.% H_2 in Ar together with 0.03 vol.% CO_2 to maintain a 1:3 molar ratio and to study the CO_2 and H_2 interactions on the surface of In_{13}/ZrO_2 and In_{13}/CeO_2. When the sample was exposed to the H_2 atmosphere, new peaks related to methoxy groups around 2850 and 2937 cm^{-1} appeared at 493 K over In_{13}/ZrO_2 (more intense) and In_{13}/CeO_2 (less intense) along with carbonate and bicarbonate species (Figure 7).[58,59] The large peak around 2334-2364 cm^{-1} is due to the presence of gas-phase CO_2. The formate species were also observed at 1620, 1380, and 2740 cm^{-1} on the surface of In_{13}/ZrO_2 and In_{13}/CeO_2.[58,59] The intensity of formate peaks was higher over In_{13}/ZrO_2 than In_{13}/CeO_2. The peaks disappeared in the case of In_{13}/CeO_2 while they became more intense over In_{13}/ZrO_2 when the temperature was increased from 493 to 553 K (Figure. 6).[60] In addition to this, various types of O-H bands between 3400-3700 cm^{-1}, which are related to bridge as well as hydrogen-bonded OH groups, were observed over In_{13}/ZrO_2 (Figure 7a). While over In_{13}/CeO_2, only two OH bands related to bridged species on Ce^{3+} and Ce^{4+} appeared at low temperatures which further disappeared at higher temperatures and only one OH band remained over the catalyst surface which is assigned to hydrogen-bonded OH groups (Figure 7b). In the DRIFT experiments, the OH bands are weak and the reason for this is likely that DRIFT experiments are run at atmospheric pressure. It is well known that CO_2 hydrogenation requires higher pressure to increase the yield. The low conversion of CO_2 and thereby the low formation of water could explain why the OH bands are small. Anyhow, OH bands are visible, and it is likely that these species would be significantly larger at real operating conditions with high pressure hydrogen. It is therefore possible that at higher H_2 pressure the O-H groups could cover the surface of In_{13}/CeO_2, which could result in low CO_2 conversion and methanol selectivity. This hypothesis is supported by the XPS data where 30.8 % metal hydroxides was found over the spent

In_{13}/CeO_2 catalyst.

The CO_2 adsorption and desorption were studied in TPD experiments for In_2O_3, In_{13}/ZrO_2 and In_{13}/CeO_2 (Figure 8). A common desorption peak was below 550 K which was due to physisorbed CO_2.[19] The peak above 550 K could be attributed to chemisorption of CO_2 from thermally induced oxygen vacancies.[18] It was difficult to distinguish the boundary between physio- and chemisorbed CO_2 peaks in the case of In_{13}/CeO_2. The total CO_2 desorbed values were 30, 181, and 191 μmol/g for In_2O_3, In_{13}/ZrO_2 and In_{13}/CeO_2, respectively. A significantly lower amount of CO_2 adsorption was found on the unsupported In_2O_3 compared to the supported catalysts, which was probably related to its substantially lower specific surface area. The total amount of CO_2 desorbed was higher on In_{13}/CeO_2 than In_{13}/ZrO_2, which might be due to more oxygen defects on In_{13}/CeO_2, which is in-line with the XPS analysis (Figure 8a).[12,61]

H_2-TPR measurements were used to study the reduction behavior of the catalysts (Figure 8b). The H_2-TPR profile of the unsupported bulk In_2O_3 exhibited two main stages of H_2 consumption. The first one was at approximately 531 K due to the reduction of the surface species while the second one started from around 798 K and the reduction was not complete even when it was prolonged at 1073 KC for 30 min. This is a typical behavior of In_2O_3 as reported in the literature [62]. The H_2-TPR profile of the In_{13}/ZrO_2 sample showed two hydrogen consumption peaks at 513 and 943 K. We note that the ZrO_2 support consumed only a negligible amount of H_2 at around 943 K (data not shown). Therefore, the reduction of the In_2O_3 component accounted mainly for the hydrogen consumption of the In_{13}/ZrO_2 catalyst. However, the first peak was shifted to a lower temperature than that of the unsupported bulk In_2O_3, suggesting that the reduction of In_2O_3 was enhanced. Furthermore, the total area of the peaks was significantly smaller than that of the bulk In_2O_3 because the In_{13}/ZrO_2 contained a lower amount of In_2O_3 than the unsupported catalyst. In_{13}/CeO_2 showed two H_2 uptakes at 531

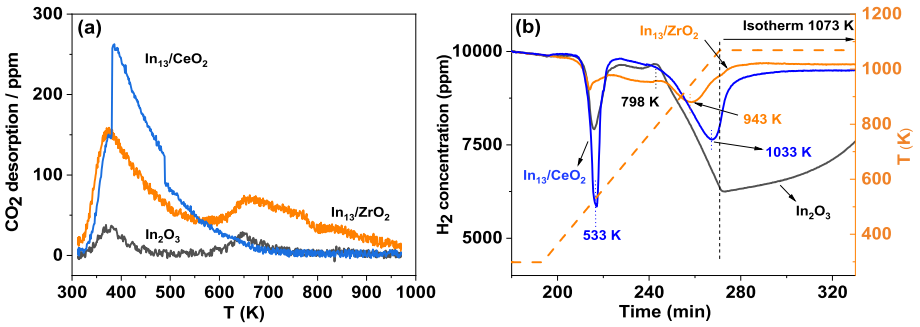

Figure 8. CO_2 TPD (a) of bulk In_2O_3, In_{13}/ZrO_2 and In_{13}/CeO_2, and H_2-TPR (b) of bulk In_2O_3 In_{13}/ZrO_2 and In_{13}/CeO_2 at atmospheric pressure.

K and 1033 K. The total area of the two peaks was significantly higher than that of the In_{13}/ZrO_2. Because both catalysts had a similar loading of In_2O_3, this suggests that CeO_2 contributed to the hydrogen consumption of the In_{13}/CeO_2 catalyst. Indeed, the CeO_2 support exhibited two peaks of hydrogen consumption. The first one started around 593 K and peaked at 843 K due to the reduction of surface CeO_2 while the second one began at approximately 953 K due to the reduction of bulk CeO_2 and it was not completed even at 1073 K for 30 min (data not shown). It should be noted that the first reduction peak (at 533 K) of the In_{13}/CeO_2 was substantially larger than that on both unsupported In_2O_3 and In_{13}/ZrO_2. This suggested that CeO_2 enhanced the reduction of In_2O_3. The quantification of H_2 consumption was not performed because the reduction was not completed for all three catalysts in the measured temperature range.

3.3. Catalytic activity

The catalytic performance of the Indium supported (In_x) on CeO_2 and ZrO_2 was assessed, where Indium loading (x) was kept at 1 % and 13 %. The In_{13}/ZrO_2 catalyst was tested at various temperatures from 493 to 573 at 3.0 MPa to examine the effect of reaction conditions on methanol synthesis (Figure 9). It was observed that the CO_2 conversion and CO selectivity increased with increasing temperature while the selectivity for CH_3OH decreased because of the competition of the RWGS reaction at high temperatures, which is in line with previous studies.[18] The In_{13}/ZrO_2 catalyst exhibited 100 % CH_3OH selectivity with 0.6 % CO_2 conversion at 493 K. Increasing the temperature to 573 K, resulted in the CO_2 conversion increasing to 12.7 %, while the CH_3OH selectivity dropped to 57.3 % and the CO selectivity was 42.3% (Figure 9). In addition, the CH_4 selectivity also increased from 0 to 0.21 % with increasing temperature from 493 to 573 K.

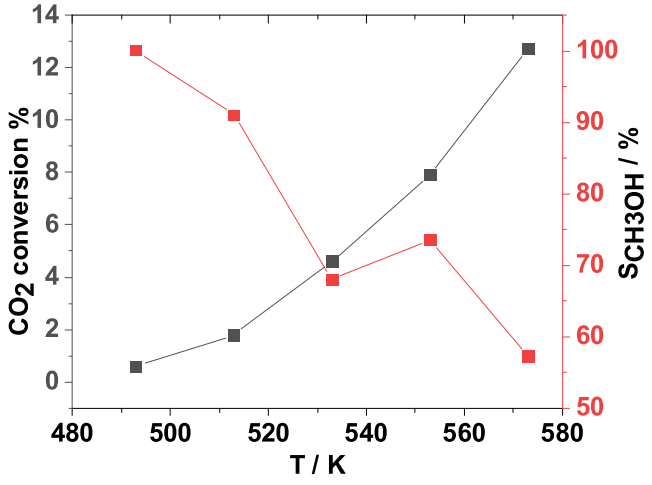

Figure 9. CO_2 hydrogenation over In_{13}/ZrO_2 at various temperatures, Reaction conditions: Catalyst= 0.5 g, feed gas molar ratio (H_2 : CO_2) = 3:1; GHSV = 12000 h^{-1} and P = 3.0 MPa.

Figure 10 shows that the combination of In_2O_3 and ZrO_2 improved significantly the CO_2 conversion as compared to its individual components. Activity measurements for each catalyst were performed at 493, 553 and 573 K. After the temperature reached the set value, the reaction was prolonged at this temperature for about 1 h while the outlet gas was continuously analyzed. We report the data near the end of this period. At 553 K, the CO_2 conversions over the unsupported bulk In_2O_3 and ZrO_2 support were negligible while it significantly increased from 0.6 % (over bulk In_2O_3) to 7.9 % over In_{13}/ZrO_2. Both samples of CeO_2-supported In catalysts showed lower conversion of CO_2 than the unsupported bulk In_2O_3 but higher than the CeO_2 support. The CO_2 conversion increased with increasing temperature over In_2O_3, ZrO_2, In_x/ZrO_2 and In_x/CeO_2. Surprisingly, the conversion decreased over CeO_2 when increasing the temperature, however, it should be noted that the conversions over CeO_2 were very low over the entire temperature span investigated. The change in CO_2 conversion over In_x/CeO_2 with increasing temperature was more moderate compared to that with In_x/ZrO_2. The low increment in the conversion of CO_2 with increasing temperature for the CeO_2-based catalysts raises some suspicion that there is a factor that makes these catalysts unstable under the operating conditions of the reaction and this will be further discussed in Section 3.8. The CO_2 conversion increased with increasing In loading from 1 % to 13 % over both supports. Thus, the further characterizations were carried out with 13 % In loading catalysts and are discussed here in detail.

The CH_3OH selectivity decreased with increasing temperature from 493 to 573 K over all catalysts due to the competition of the RWGS reaction at high temperatures. Notably, methanol was the main product when the In loading was 13 % while CO was the main product with 1 % In loading at 573 K for both the supported catalysts. At 493 K, the selectivity for CH_3OH increased from 68 % to 85 % as the loading of In increased from 1 % to 13 %. Wang et al. found that the activity of bulk ZrO_2 was negligible, with only 0.18 % CO_2 conversion at 573 K.[13] The CH_4 selectivity also increased with increasing temperature over all catalysts from 493 to 573 K. Additionally, In_x/CeO_2 exhibited higher selectivity towards CH_4 than In_x/ZrO_2 for both In loadings. The CeO_2 exhibited negligible conversion. After loading In over CeO_2, it became active toward methanol synthesis. Further, the CH_3OH selectivity decreased, and the CO selectivity increased over In_x/CeO_2, when the temperature increased from 493 to 573 K. The change in selectivity for CH_3OH and CO was much less when In loading was 13 %. The In_x/CeO_2 showed higher methanol selectivity as compared to In_x/ZrO_2 with both levels of In loading at 553 and 573 K. However, the maximum methanol STY at 553 K and 3.0 MPa was 0.17 and 0.007 $g_{MeOH}\ h^{-1}\ g_{cat}^{-1}$ over In_{13}/ZrO_2 and In_{13}/CeO_2, respectively.

3.4. Catalyst stability

Stability is a key factor to determine the use of catalysts for CH_3OH synthesis from CO_2 hydrogenation on an industrial scale. The stability

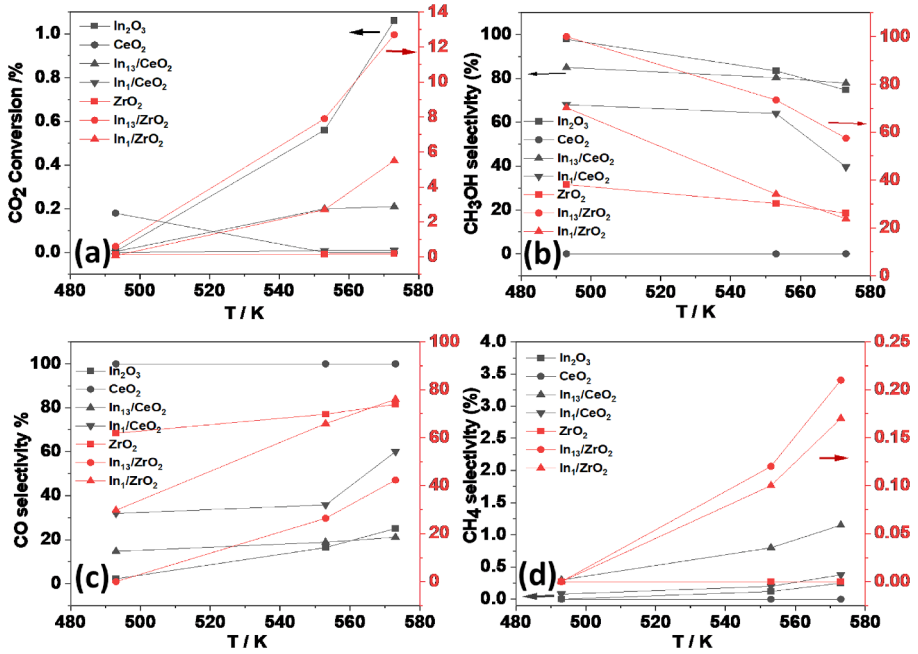

Figure 10. CO_2 hydrogenation over In_2O_3, In_{13}/ZrO_2, In_{13}/CeO_2, In_1/ZrO_2, In_1/CeO_2, ZrO_2 and CeO_2 (a) CO_2 conversion and (b) CH_3OH selectivity, (c) CO selectivity and, (d) CH_4 selectivity, Reaction conditions: Catalyst= 0.5 g, feed gas ratio (H_2 : CO_2)=3:1, P = 3.0 MPa and, GHSV = 12000 h^{-1}.

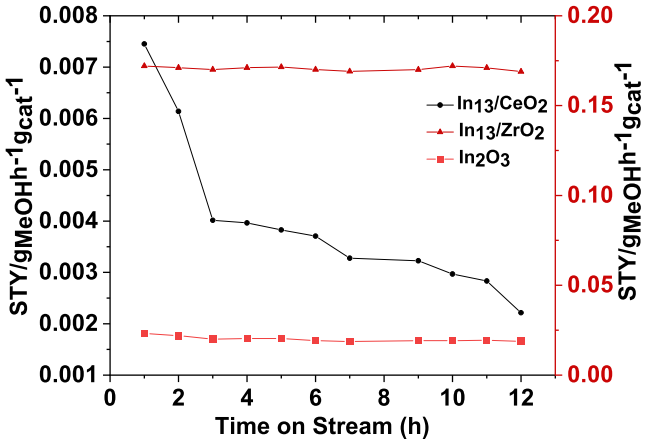

Figure 11. Evolution of the methanol STY with time on stream (TOS) over In_{13}/ZrO_2 and In_{13}/CeO_2. Reaction conditions: Catalyst= 0.5 g, feed molar gas ratio (H_2 : CO_2)=3:1, P = 3.0 MPa and, GHSV = 12000 h^{-1}, T = 553 K.

test of bulk In_2O_3, In_{13}/ZrO_2 and In_{13}/CeO_2 was performed at 553 K and 3.0 MPa because the catalysts exhibited the best STY of methanol at this condition. Figure 11 compares the methanol STY versus the time-on-stream over bulk In_2O_3, In_{13}/ZrO_2 and In_{13}/CeO_2. The In_{13}/ZrO_2 and bulk In_2O_3 catalysts were found to be stable for the entire duration of 12 h, whereas methanol STY of In_{13}/CeO_2 decreased dramatically from the beginning to 2 h of time-on-stream and then dropped steadily till the end of the test at 12 h. Further, the stability test for In_{13}/ZrO_2 was prolonged and the methanol STY was stable up to 50 h of time-on-stream (Figure S7). The deactivation will be discussed in Section 4.

4. Discussion

The selectivity for CH_3OH was higher for In_{13}/CeO_2 than In_{13}/ZrO_2 at 553 K while the STY for CH_3OH was higher over In_{13}/ZrO_2 than In_{13}/CeO_2. The positive effect of CeO_2 in CO_2 hydrogenation has been reported in terms of CH_3OH selectivity when ZrO_2 was partially replaced by CeO_2.[63] In the DRIFT study, more bi-carbonates, formats, and methoxy species were observed over In_{13}/ZrO_2. The higher activity of In_{13}/ZrO_2 than our unsupported bulk In_2O_3 is likely due to the significantly higher surface area. In addition, we observed an interaction between ZrO_2 and In_2O_3 in XRD and it has been reported that this interaction increased the stability of various intermediates like $*CO_2$, *CO, *HCO, and $*H_2CO$ which could give a higher activity of In_{13}/ZrO_2. [25,64]

During the reaction period, the STY of CH_3OH was constant for In_{13}/ZrO_2 while it approached zero for In_{13}/CeO_2 with time. These results show that the In_{13}/CeO_2 catalyst deactivated after 12 h on stream. Similar deactivation has been observed in the case of a Pd/CeO_2 catalyst for CO_2 hydrogenation.[65] To further understand the deactivation of In_{13}/CeO_2, we have characterized the catalyst before and after reaction (spent catalyst) using XRD, N_2 physisorption and XPS. The XRD measurements (Figure 1) revealed that the crystallite size of the ceria support increased in the spent catalyst, which is a sign of sintering of the support material. Moreover, the specific surface area also decreased from 66 to 48 m^2/g which also suggests that the support sintered during the reaction. Interestingly, the XPS data also revealed that the $In(OH)_3$ species were still present over spent In_{13}/CeO_2 while they disappeared in the spent In_{13}/ZrO_2 (Figure S6a). Moreover, the In^0/In_2O_3 ratio also changed significantly differently between In_{13}/ZrO_2 and In_{13}/CeO_2 after the reaction. The ratio of In^0/In_2O_3 increased 2.2-fold for In_{13}/ZrO_2 whereas it decreased by 2.6-fold for In_{13}/CeO_2. This suggested that In_2O_3 in In_{13}/ZrO_2 was reduced further while metallic In in In_{13}/CeO_2 was partially oxidized after the reaction. Furthermore, it was also noted that more Ce^{3+} was present in the spent In_{13}/CeO_2 while a small fraction of Zr^0 was also detected for the spent In_{13}/ZrO_2. This indicated that the supports (CeO_2 and ZrO_2) were partially reduced after the hydrogenation reaction; however, the reduction of CeO_2 is easier than ZrO_2 to some extent as also observed from H_2-TPR. A redox pair of Ce^{3+}/Ce^{4+} and In^0/In^{3+} may explain an increase in the amount of Ce^{3+} and a decrease in the amount of In^0 in the In_{13}/CeO_2 after the reaction, and this is in line with the H_2-TPR data. Also, from DRIFTs measurements OH groups were visible although at low levels, likely due to low conversion and low water formation in the DRIFT experiments since they were performed at atmospheric pressure. Here, water should play a crucial role in the

deactivation of the catalyst as it is a side product of CO_2 hydrogenation. Therefore it might be possible that the produced water can deactivate the active sites of the catalyst.[65] It has been reported and confirmed that CeO_2 is a good absorbent for water molecules due to its hydrophilic nature and a very stable configuration of water has been observed on the surface of CeO_2.[37]

It was also observed in the DRIFT study that the bands related to methoxy, formate and carbonate species disappeared at higher temperature over In_{13}/CeO_2, indicating less adsorption of CO_2 molecules over CeO_2 at higher temperature.[66,67] However, the presence of water molecules around the In surface could create a physical hindrance for the CO_2 molecules and also cause sintering of In. [18]

To summarize, In_{13}/CeO_2 has a high initial selectivity for methanol production, but it rapidly deactivates with time on stream. In_{13}/ZrO_2 on the other hand exhibited a stable methanol production during the 50 h long experiment. The deactivation of In_{13}/CeO_2 is likely linked to a sintering of support which caused lower surface area and the redox property of CeO_2 which induced the oxidation of metallic In.

4.1. Regeneration of In/CeO_2

In_{13}/ZrO_2 catalysts were found to be stable at 533 K and 3.0 MPa whereas the In_{13}/CeO_2 catalyst showed severe deactivation after only a few hours of time on stream. A regeneration study of In_{13}/CeO_2 was therefore carried out at 533 K and 3.0 MPa to determine the type of deactivation (Figure 12). After the reaction, the catalyst was flushed with Ar (50 Nml/min), while the reactor was cooled from reaction temperature to room temperature and further maintained in Ar flow overnight. The next day, the Ar flow was switched to reactant feed and the temperature was increased from room temperature to reaction temperature. It was observed that the STY for methanol decreased during the first day under reaction conditions. Further, the catalyst bed was flushed and tested again on the second day at the same reaction conditions. The STY was partially recovered from the previous day but again started to decrease with time. This process was again repeated on the third day and a similar phenomenon was observed, although at significantly lower STY levels. It can be stated that some part of deactivation is reversible as the STY increased after flushing with Ar. Thus, due to the strong hydrophilic character of the CeO_2 carrier, significant amounts of water form and assemble on the catalyst during the reaction. The water could inhibit CO_2 hydrogenation, and we suggest that it could be partly removed after Ar flushing from the CeO_2 surface and thereby increasing the CO_2 adsorption and methanol formation. However, the decreased surface area is not reversible, and the catalyst could therefore not gain the original state back, which could be the reason behind the continuous overall deactivation of the catalyst over the three days observed in Figure 12.

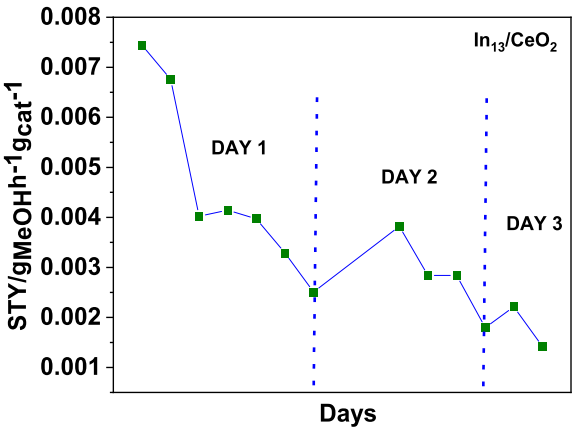

Figure 12. Regeneration study of In_{13}/CeO_2 . Reaction conditions: Catalyst= 0.5 g, feed gas ratio (H_2 : CO_2) = 3:1, P = 3.0 MPa and, GHSV = 12000 h^{-1}, T = 553 K. Between each day the catalyst was flushed and cooled in Ar and then kept in Ar flow over night.

5. Conclusions

To uncover the effect of ZrO_2 and CeO_2 supports on In_2O_3 activity in the hydrogenation of CO_2 to methanol, In_2O_3 supported on ZrO_2 and CeO_2 catalysts were prepared. The selectivity for CH_3OH was higher for In_{13}/CeO_2 than In_{13}/ZrO_2 at 553 K, but the CH_3OH yield was higher over In_{13}/ZrO_2. For the In_{13}/ZrO_2 the CO_2 conversion and CO selectivity increased with increasing temperature while the selectivity for CH_3OH decreased. In addition, some methane was formed, which increased with temperature. A large drawback with the In_{13}/CeO_2 sample was that it deactivated severely with time on stream and already after 2 h a significant deactivation was observed. In_{13}/ZrO_2, on the other hand, exhibited a stable behavior during 50 h on stream. The spent catalysts were characterized to understand the different behavior of In_{13}/CeO_2 than In_{13}/ZrO_2 during the time on stream. The XPS results revealed that during the reaction the ratio of In^0/In_2O_3 increased from 0.29 to 0.65 for the In_{13}/ZrO_2 whereas it decreased from 0.88 to 0.34 for the In_{13}/CeO_2. The data suggest that the redox property of CeO_2 (Ce^{3+} ion increased from 18 to 45 % in the spent In_{13}/CeO_2) induced the oxidation of metallic In and increased the amount of In_2O_3. Moreover, the percentage of $In(OH)_3$ was 30.8 % over the spent In_{13}/CeO_2 whereas it became zero over the spent In_{13}/ZrO_2. In addition, OH groups were found during DRIFT experiments, although at low levels likely due to that the experiments were performed at atmospheric pressure, resulting in low conversion and thereby low water production. We, therefore, propose that the water produced during reaction results in the formation of hydroxyls on the In_{13}/CeO_2, which was one of the deactivating factors. However, this is not the main reason for the deactivation, because XRD experiments showed that the sintering of CeO_2 support (larger crystallite size) for the spent In_{13}/CeO_2 catalyst. In addition, the specific surface area also decreased due to sintering, while it remained the same for In_{13}/ZrO_2. Thus, the structural changes, presence of more OH groups (hydrophilic nature) and the decreased surface area of spent In_{13}/CeO_2 after the reaction are the reasons for the decreased activity. Further, a regeneration study of In_{13}/CeO_2 was conducted and that revealed that the catalyst can be regenerated to some extent by flushing the catalyst with Ar. However, repeated reaction-regeneration cycles revealed that the conversion continued to decrease after the regeneration and was even lower after subsequent cycles. To conclude, the water adsorption on In_{13}/CeO_2 is partly reversible and the catalyst can therefore gain back some activity after Ar flushing, but the structural changes are not reversible and cause a continuous deactivation. In_{13}/ZrO_2, on the other hand, exhibited a stable behavior during the reaction conditions used in this study.

CRediT authorship contribution statement

Poonam Sharma: Conceptualization, Data curation, Formal analysis, Investigation, Visualization, Writing – original draft, Methodology. **Phuoc Hoang Ho:** Data curation, Formal analysis, Methodology, Validation, Visualization, Writing – review & editing. **Jieling Shao:** Data curation, Formal analysis, Validation. **Derek Creaser:** Conceptualization, Formal analysis, Methodology, Supervision, Writing – review & editing. **Louise Olsson:** Formal analysis, Funding acquisition, Methodology, Project administration, Supervision, Writing – review & editing.

Declaration of Competing Interest

The authors declare that they have no known competing financial interests or personal relationships that could have appeared to influence the work reported in this paper.

Data availability

Data will be made available on request.

Acknowledgements

We would like to acknowledge the funding from Swedish Energy Agency (P47450-1). We are thankful to Saint-Gobain NORPRO for providing catalyst support material for this work.

Appendix A. Supplementary data

Supplementary data to this article can be found online at https://doi.org/10.1016/j.fuel.2022.125878.

References

[1] Rogelj J, Den Elzen M, Höhne N, Fransen T, Fekete H, Winkler H, et al. Paris Agreement climate proposals need a boost to keep warming well below 2 C. Nature 2016;534(7609):631–9.
[2] Davis SJ, Caldeira K, Matthews HD. Future CO2 emissions and climate change from existing energy infrastructure. Science 2010;329(5997):1330–3.
[3] Song C. Global challenges and strategies for control, conversion and utilization of CO2 for sustainable development involving energy, catalysis, adsorption and chemical processing. Catalysis today 2006;115(1–4):2–32.
[4] Olah GA, Prakash GS, Goeppert A. Anthropogenic chemical carbon cycle for a sustainable future. Journal of the American Chemical Society 2011;133(33):12881–98.
[5] Chen Y, Choi S, Thompson LT. Low temperature CO2 hydrogenation to alcohols and hydrocarbons over Mo2C supported metal catalysts. Journal of Catalysis 2016;343:147–56.
[6] Álvarez A, Bansode A, Urakawa A, Bavykina AV, Wezendonk TA, Makkee M, et al. Challenges in the greener production of formates/formic acid, methanol, and DME by heterogeneously catalyzed CO2 hydrogenation processes. Chemical reviews 2017;117(14):9804–38.
[7] Sharma P, Sebastian J, Ghosh S, Creaser D, Olsson L. Recent advances in hydrogenation of CO 2 into hydrocarbons via methanol intermediate over heterogeneous catalysts. Catalysis Science & Technology 2021;11(5):1665–97.
[8] Jiang X, Nie X, Guo X, Song C, Chen JG. Recent advances in carbon dioxide hydrogenation to methanol via heterogeneous catalysis. Chemical reviews 2020;120(15):7984–8034.
[9] Sun K, Fan Z, Ye J, Yan J, Ge Q, Li Y, et al. Hydrogenation of CO2 to methanol over In2O3 catalyst. Journal of CO2 Utilization 2015;12:1–6.
[10] Luo W, Xie W, Li M, Zhang J, Züttel A. 3D hierarchical porous indium catalyst for highly efficient electroreduction of CO 2. Journal of Materials Chemistry A 2019;7(9):4505–15.
[11] Rui N, Wang Z, Sun K, Ye J, Ge Q, Liu C-j. CO2 hydrogenation to methanol over Pd/In2O3: effects of Pd and oxygen vacancy. Applied Catalysis B: Environmental 2017;218:488–97.
[12] Frei MS, Mondelli C, García-Muelas R, Kley KS, Puértolas B, López N, et al. Atomic-scale engineering of indium oxide promotion by palladium for methanol production via CO 2 hydrogenation. Nature communications 2019;10(1).
[13] Wang J, Li G, Li Z, Tang C, Feng Z, An H, et al. A highly selective and stable ZnO-ZrO2 solid solution catalyst for CO2 hydrogenation to methanol. Science advances 2017;3(10):e1701290.
[14] Richard AR, Fan M. The effect of lanthanide promoters on NiInAl/SiO2 catalyst for methanol synthesis. Fuel 2018;222:513–22.
[15] Akkharaphatthawon N, Chanlek N, Cheng CK, Chareonpanich M, Limtrakul J, Witoon T. Tuning adsorption properties of GaxIn2− xO3 catalysts for enhancement of methanol synthesis activity from CO2 hydrogenation at high reaction temperature. Applied Surface Science 2019;489:278–86.
[16] Richard AR, Fan M. Low-pressure hydrogenation of CO2 to CH3OH using Ni-In-Al/SiO2 catalyst synthesized via a phyllosilicate precursor. ACS Catalysis 2017;7(9):5679–92.
[17] Frei MS, Capdevila-Cortada M, García-Muelas R, Mondelli C, López N, Stewart JA, et al. Mechanism and microkinetics of methanol synthesis via CO2 hydrogenation on indium oxide. Journal of Catalysis 2018;361:313–21.
[18] Martin O, Martín AJ, Mondelli C, Mitchell S, Segawa TF, Hauert R, et al. Indium oxide as a superior catalyst for methanol synthesis by CO2 hydrogenation. Angewandte Chemie International Edition 2016;55(21):6261–5.
[19] Chen T-Y, Cao C, Chen T-B, Ding X, Huang H, Shen L, et al. Unraveling Highly Tunable Selectivity in CO2 Hydrogenation over Bimetallic In-Zr Oxide Catalysts. ACS Catalysis 2019;9(9):8785–97.
[20] Yao L, Shen X, Pan Y, Peng Z. Synergy between active sites of Cu-In-Zr-O catalyst in CO2 hydrogenation to methanol. Journal of Catalysis 2019;372:74–85.
[21] Behrens M, Studt F, Kasatkin I, Kühl S, Hävecker M, Abild-Pedersen F, et al. The active site of methanol synthesis over Cu/ZnO/Al2O3 industrial catalysts. Science 2012;336(6083):893–7.
[22] Mikkelsen M, Jørgensen M, Krebs FC. The teraton challenge. A review of fixation and transformation of carbon dioxide. Energy. Environ Sci 2010;3(1):43–81.
[23] Jadhav SG, Vaidya PD, Bhanage BM, Joshi JB. Catalytic carbon dioxide hydrogenation to methanol: a review of recent studies. Chem Eng Res Des 2014;92(11):2557–67.
[24] Wu J, Saito M, Takeuchi M, Watanabe T. The stability of Cu/ZnO-based catalysts in methanol synthesis from a CO2-rich feed and from a CO-rich feed. Appl Catal, A 2001;218(1–2):235–40.
[25] Yang C, Pei C, Luo R, Liu S, Wang Y, Wang Z, et al. Strong electronic oxide–support interaction over In2O3/ZrO2 for highly selective CO2 hydrogenation to methanol. Journal of the American Chemical Society 2020;142(46):19523–31.
[26] Hartadi Y, Widmann D, Behm RJ. CO2 hydrogenation to methanol on supported Au catalysts under moderate reaction conditions: support and particle size effects. ChemSusChem 2015;8(3):456–65.
[27] Wambach J, Baiker A, Wokaun A. CO 2 hydrogenation over metal/zirconia catalysts. Physical Chemistry Chemical Physics 1999;1(22):5071–80.
[28] Arena F, Barbera K, Italiano G, Bonura G, Spadaro L, Frusteri F. Synthesis, characterization and activity pattern of Cu–ZnO/ZrO2 catalysts in the hydrogenation of carbon dioxide to methanol. Journal of Catalysis 2007;249(2):185–94.
[29] Gao P, Li F, Zhan H, Zhao N, Xiao F, Wei W, et al. Influence of Zr on the performance of Cu/Zn/Al/Zr catalysts via hydrotalcite-like precursors for CO2 hydrogenation to methanol. Journal of catalysis 2013;298:51–60.
[30] Guo X, Mao D, Lu G, Wang S, Wu G. Glycine–nitrate combustion synthesis of CuO–ZnO–ZrO2 catalysts for methanol synthesis from CO2 hydrogenation. Journal of Catalysis 2010;271(2):178–85.
[31] Li K, Chen JG. CO2 hydrogenation to methanol over ZrO2-containing catalysts: Insights into ZrO2 induced synergy. ACS Catalysis 2019;9(9):7840–61.
[32] Frei MS, Mondelli C, Cesarini A, Krumeich F, Hauert R, Stewart JA, et al. Role of zirconia in indium oxide-catalyzed CO2 hydrogenation to methanol. ACS Catalysis 2020;10(2):1133–45.
[33] Zhao B, Pan Y-X, Liu C-J. Liu C-j. The promotion effect of CeO2 on CO2 adsorption and hydrogenation over Ga2O3. Catalysis Today 2012;194(1):60–4.
[34] Reddy BM, Reddy GK, Katta L. Structural characterization and dehydration activity of CeO2–SiO2 and CeO2–ZrO2 mixed oxides prepared by a rapid microwave-assisted combustion synthesis method. Journal of Molecular Catalysis A: Chemical 2010;319(1–2):52–7.
[35] Wang B, Wu X, Ran R, Si Z, Weng D. IR characterization of propane oxidation on Pt/CeO2–ZrO2: The reaction mechanism and the role of Pt. Journal of Molecular Catalysis A: Chemical 2012;356:100–5.
[36] Porosoff MD, Chen JG. Trends in the catalytic reduction of CO2 by hydrogen over supported monometallic and bimetallic catalysts. Journal of catalysis 2013;301:30–7.
[37] Wang W, Zhang Y, Wang Z, Yan J-M, Ge Q, Liu C-J. Liu C-j. Reverse water gas shift over In2O3–CeO2 catalysts. Catal Today 2016;259:402–8.
[38] Li W, Huang H, Li H, Zhang W, Liu H. Facile synthesis of pure monoclinic and tetragonal zirconia nanoparticles and their phase effects on the behavior of supported molybdena catalysts for methanol-selective oxidation. Langmuir 2008;24(15):8358–66.
[39] Gao P, Zhang L, Li S, Zhou Z, Sun Y. Novel heterogeneous catalysts for CO2 hydrogenation to liquid fuels. ACS Central Science 2020;6(10):1657–70.
[40] Sifontes A, Gonzalez G, Ochoa J, Tovar L, Zoltan T, Cañizales E. Chitosan as template for the synthesis of ceria nanoparticles. Materials Research Bulletin 2011;46(11):1794–9.
[41] Aguilar J, Rodríguez J, Hinojosa M. Microwaves as an energy source for producing β-SiC. Journal of microwave power and electromagnetic energy 2001;36(3):169–77.
[42] Nhut J-M, Pesant L, Keller N, Pham-Huu C, Ledoux MJ. Pd/SiC exhaust gas catalyst for heavy-duty engines: improvement of catalytic performances by controlling the location of the active phase on the support. Topics in catalysis 2004;30(1–4):353–8.
[43] Trung HM, Thien ND, Lien DT, Long NN. Synthesis and characterization of indium nanoparticles. VNU Journal of Science: Mathematics-Physics 2011;27(3):147–53.
[44] Thommes M, Kaneko K, Neimark AV, Olivier JP, Rodriguez-Reinoso F, Rouquerol J, et al. Physisorption of gases, with special reference to the evaluation of surface area and pore size distribution (IUPAC Technical Report). Pure and applied chemistry 2015;87(9-10):1051-69.
[45] Dupin J-C, Gonbeau D, Vinatier P, Levasseur A. Systematic XPS studies of metal oxides, hydroxides and peroxides. Physical Chemistry Chemical Physics 2000;2(6):1319–24.
[46] Hoch LB, Wood TE, O'Brien PG, Liao K, Reyes LM, Mims CA, et al. The Rational Design of a Single-Component Photocatalyst for Gas-Phase CO2 Reduction Using Both UV and Visible Light. Advanced Science 2014;1(1):1400013.
[47] Huang C, Tang Z, Zhang Z. Differences between zirconium hydroxide (Zr (OH) 4· nH2O) and hydrous zirconia (ZrO2· nH2O). Journal of the American Ceramic Society 2001;84(7):1637–8.
[48] Lackner P, Zou Z, Mayr S, Diebold U, Schmid M. Using photoelectron spectroscopy to observe oxygen spillover to zirconia. Physical Chemistry Chemical Physics 2019;21(32):17613–20.
[49] Li W, Nie X, Jiang X, Zhang A, Ding F, Liu M, et al. ZrO2 support imparts superior activity and stability of Co catalysts for CO2 methanation. Applied Catalysis B: Environmental 2018;220:397–408.
[50] Xu L, Song H, Dong B, Wang Y, Chen J, Bai X. Preparation and bifunctional gas sensing properties of porous In2O3− CeO2 binary oxide nanotubes. Inorganic chemistry 2010;49(22):10590–7.
[51] Zhou Y, Perket JM, Zhou J. Growth of Pt nanoparticles on reducible CeO2 (111) thin films: effect of nanostructures and redox properties of ceria. The Journal of Physical Chemistry C 2010;114(27):11853–60.

[52] Chen Z, Kronawitter CX, Yang X, Yeh Y-w, Yao N, Koel BE. The promoting effect of tetravalent cerium on the oxygen evolution activity of copper oxide catalysts. Physical Chemistry Chemical Physics 2017;19(47):31545–52.
[53] Garcia X, Soler L, Divins NJ, Vendrell X, Serrano I, Lucentini I, et al. Ceria-based catalysts studied by near ambient pressure x-ray photoelectron spectroscopy: a review. Catalysts 2020;10(3):286.
[54] Detweiler ZM, Wulfsberg SM, Frith MG, Bocarsly AB, Bernasek SL. The oxidation and surface speciation of indium and indium oxides exposed to atmospheric oxidants. Surface Science 2016;648:188–95.
[55] Thomas III J, Kaganowicz G, Robinson J. X-ray Photoelectron Spectroscopy Analysis of Changes in InP and InGaAs Surfaces Exposed to Various Plasma Environments. Journal of The Electrochemical Society 1988;135(5):1201–7.
[56] Pokrovski K, Jung KT, Bell AT. Investigation of CO and CO2 adsorption on tetragonal and monoclinic zirconia. Langmuir 2001;17(14):4297–303.
[57] Hertl W. Surface chemistry of zirconia polymorphs. Langmuir 1989;5(1):96–100.
[58] Ni Y, Chen Z, Fu Y, Liu Y, Zhu W, Liu Z. Selective conversion of CO 2 and H 2 into aromatics. Nature communications 2018;9(1):1–7.
[59] Li Z, Qu Y, Wang J, Liu H, Li M, Miao S, et al. Highly selective conversion of carbon dioxide to aromatics over tandem catalysts. Joule 2019;3(2):570–83.
[60] Hemmingsson F, Schaefer A, Skoglundh M, Carlsson P-A. CO2 Methanation over Rh/CeO2 Studied with Infrared Modulation Excitation Spectroscopy and Phase Sensitive Detection. Catalysts 2020;10(6):601.
[61] Glorius M, Markovits MA, Breitkopf C. Design of specific acid-base-properties in CeO2-ZrO2-mixed oxides via templating and Au modification. Catalysts 2018;8(9):358.
[62] Chou C-Y, Lobo RF. Direct conversion of CO2 into methanol over promoted indium oxide-based catalysts. Applied Catalysis A: General 2019;583:117144.
[63] Bonura G, Arena F, Mezzatesta G, Cannilla C, Spadaro L, Frusteri F. Role of the ceria promoter and carrier on the functionality of Cu-based catalysts in the CO2-to-methanol hydrogenation reaction. Catalysis Today 2011;171(1):251–6.
[64] Kattel S, Yan B, Yang Y, Chen JG, Liu P. Optimizing binding energies of key intermediates for CO2 hydrogenation to methanol over oxide-supported copper. Journal of the American Chemical Society 2016;138(38):12440–50.
[65] Fan L, Fujimoto K. Development of an active and stable ceria-supported palladium catalyst for hydrogenation of carbon dioxide to methanol. Applied Catalysis A: General 1993;106(1):L1–7.
[66] Li M, Tumuluri U, Wu Z, Dai S. Effect of dopants on the adsorption of carbon dioxide on ceria surfaces. ChemSusChem (Online) 2015;8(21):3651–60.
[67] Hahn KR, Iannuzzi M, Seitsonen AP, Jr H. Coverage effect of the CO2 adsorption mechanisms on CeO2 (111) by first principles analysis. The Journal of Physical Chemistry C 2013;117(4):1701–11.